World Academy of Science, Engineering and Technology
International Journal of Civil and Environmental Engineering
Vol:17, No:1, 2023

Frequency Modulation in Vibro-Acoustic Modulation Method

D. Liu, D. M. Donskoy

***Abstract*—**The vibroacoustic modulation method is based on the modulation effect of high-frequency ultrasonic wave (carrier) by low-frequency vibration in the presence of various defects, primarily contact-type such as cracks, delamination, etc. The presence and severity of the defect are measured by the ratio of the spectral sidebands and the carrier in the spectrum of the modulated signal. This approach, however, does not differentiate between amplitude and frequency modulations, AM and FM, respectfully. This paper is an attempt to explain the generation mechanisms of FM and its correlation with the flaw properties. Here we proposed two possible mechanisms leading to FM modulation based on nonlinear local defect resonance and dynamic acoustoelastic models.

***Keywords*—**Non-destructive testing, nonlinear acoustics, structural health monitoring, acoustoelasticity, local defect resonance.

I. Introduction

In last two decades, the Vibro-Acoustic Modulation (VAM) method gained increasing interest due to its sensitivity to tiny defect. This method utilizes nonlinear interaction (modulation) of a high frequency ultrasonic wave (carrier signal) having frequency ω and a low frequency sound wave (modulating vibration) with frequency $\Omega \ll \omega$ [1]-[5]. The modulation is taking place in the presence of various flaws such as fatigue and stress-corrosion cracks, disbonds, etc., Fig. 1. The most common cause of a flaw's nonlinear behavior is the contact-type interfaces within these defects, though there are several other nonlinear mechanisms have been proposed, such as hysteretic, thermo-elasticity and nonlinear dissipation [2].

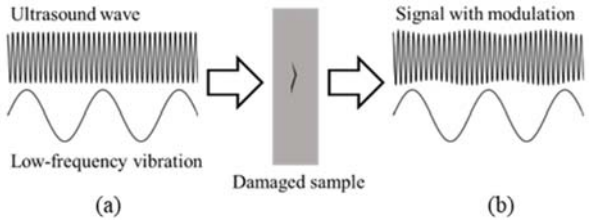

Fig. 1 Schematic representation of VAM method: The input signal (a) is a combination of a high-frequency wave (probe wave) and a low-frequency wave (pump wave); the output signal (b) will be a modulated signal with a low frequency component which can be filtered out

Most of the reported VAM studies [1]-[5] correlate flaw presence and its growth with the increase in the Modulation Index (MI) which is defined by [1]-[5]:

$$\mathrm{MI} = 20\log_{10}\frac{A_{\omega-\Omega}+A_{\omega+\Omega}}{2A_{\omega}} \quad (1)$$

where A_ω is the magnitude carrier component in the spectrum and $A_{\omega\pm\Omega}$ are the magnitude of its first sidebands. MI is the index used for describing the AM intensity of the signal, however, the higher order sidebands, as shown in Fig. 2, ($A_{\omega\pm n\Omega}$, n = 2, 3, 4…) indicate that the modulation may be more complex to include phase/frequency modulation as well. The conventional VAM method does not distinguish between AM and FM. Separate evaluation and monitoring of AM and FM could be very beneficial in understanding of flaw evolution mechanisms, separating defect-related nonlinearity from structural and material nonlinearities, improving sensitivity and reliability of the VAM method [6]. However, just a few papers [6], [7] addressed FM/AM separation in VAM testing as it is assumed that the dominant modulation mechanism is AM. The experimental results presented in [6] clearly indicate the presence of the FM which could be dominant modulation at least in the initial flaw progression. In this paper, we introduce two possible FM flaw-related mechanisms: nonlinear local defect resonance and acoustoelastic FM generation.

Frequency Modulation Due to Local Defect Resonance

A. Local Defect Resonance

Solodov introduced the concept of Local Defect Resonance (LDR) [9], [10], which treats the defect as an oscillator. When the structure is forced by an external dynamic load whose frequency is close to the resonance of the local defect, the energy of vibration will be effectively transmitted to the local defect area and lead the local defect-oscillator to a distinguishable resonating response in the vicinity of the defect. A considerable literature on LDR had grown around the study of the flat-bottomed hole (FBH), Fig. 3 [10]-[12]. FBH model is utilized for simulating a typical defect that often exists in composite materials due to delamination.

D. Liu is a graduate student with the Department of Civil, Environmental & Ocean Engineering, Stevens institute of technology, Hoboken, NJ 07030 USA (corresponding author, phone: 2017554077; e-mail: dliu20@stevens.edu).

D. M. Donskoy is a professor at the Department of Civil, Environmental & Ocean Engineering, Stevens institute of technology, Hoboken, NJ 07030 USA.

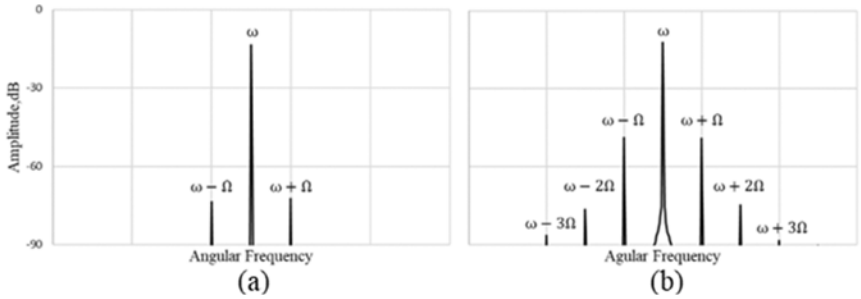

Fig. 2 Spectrum of signal that acquired from a sample at its undamaged stage (a) and its damaged stage (b). The sidebands of the intact sample are due to the structural/material nonlinearity; the increase in the amplitude of the first sideband is the evidence of the damage within the structure

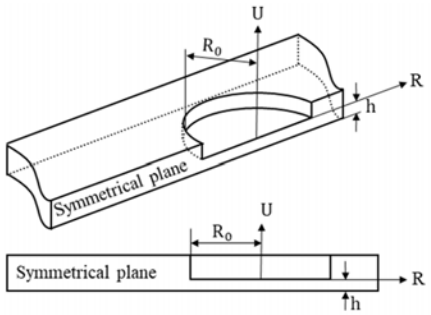

Fig. 3 Sketch of the FBH

FBH can be considered as a circular plate with a thickness of h and a radius of R_0. The boundary condition along its edges is clamped (no rotation nor displacement) [8]. The integration of the displacement of the lowest vibration mode of the plate over its surface is defined as the effective displacement U_{eff}. We substitute effective displacement U_{eff}, the kinetic energy W_K and potential energy W_P of the plate that calculated by the plate theory [13] into (2):

$$W_K = \frac{m_{eff}U_{eff}^2}{2}, W_P = \frac{k_{eff}U_{eff}^2}{2} \quad (2)$$

where k_{eff} and m_{eff} are oscillator's effective stiffness and effective mass, respectively, therefore FBH angular resonance frequency equals to:

$$f_{LDR} = \frac{1}{2\pi}\sqrt{\frac{k_{eff}}{m_{eff}}} \quad (3)$$

Numerous numerical simulations and experimental studies confirmed the analytical estimation of the FBH [10]-[12]. Additionally, it was found that the concept of LDR can also be applied to other types of defects, such as impact damages and crack type defects [12]-[14]. Although these experimental results demonstrated that crack damage could be detectable using LDR resonance response, FBH model (relying of the bending resonance of relatively thin bottom plate with thickness h, Fig. 3), may not be appropriate for these type of defect in voluminous materials (no bottom plate). Therefore, the LDR mechanism for defects within voluminous material cannot rely on bottom plate resonance and yet to be proved in simulations. We assume that a defect in unbounded media may still behave as an oscillator whose effective stiffness is determined by the defect compliance, while the effective mass is due to entrained oscillating material mass in the vicinity of the defect (similar to an oscillating bubble in fluid).

We will use numerical simulation using *COMSOL/the Solid Mechanics (Elastic Waves) interface/Frequency Domain* for a defect which is embedded inside a large volume of material with none- or low-reflective boundaries, as shown in Fig. 4.

Assuming that the defect has a circular shape with a radius "*a*", if the defect (crack) is open, it will resemble an oblate spheroidal cavity. The ratio of the major axis b and the minor axis a is called the axis ratio (AR). When the applied tensile load is changing, the AR of the cavity will be changing accordingly. Let us first consider a case that AR = 1, the shape of the cavity is spherical. The characteristic frequency of a spherical cavity in the infinite material that is [14]:

$$f_{sphere} = \frac{c_s}{\pi a} \quad (4)$$

where c_s is the shear wave velocity in surrounding material, and *a* is the sphere's radius. As the AR increases, the shape of the cavity would be altered from sphere to oblate spheroid, and the value of the characteristic frequency will decrease [15].

Numerical modeling and simulation were conducted by using the COMSOL Multiphysics *–the Solid Mechanics interface (Elastic Waves)/Frequency Domain*. The semi-infinite material is simulated by a cylinder with a roller side boundary condition, Fig. 5. Only the vertical displacement (the displacement along the direction of the plane wave propagates) is allowed. The plane wave is generated by the prescribed displacement on the top and will be damped out at the bottom by the low-reflecting boundary condition.

The material is steel with Young's modulus E = 200 GPa, density ρ = 7850 kg/m^3. The elongation in the vertical direction of an infinitesimal volume inside the semi-infinite material is accompanied by horizontal shortening due to the Poisson's effect. Because horizontal displacement is prohibited in an infinite material, a vertical propagating plane wave will cause horizontal stress, which does not exist in a practical structure with free boundary conditions. A compromising approach for simulating the plane wave in infinite material is to use a Poisson's ratio that is close to 0.5 so that the bulk modulus of

the material is extremely large, and the vertical stress is then negligible.

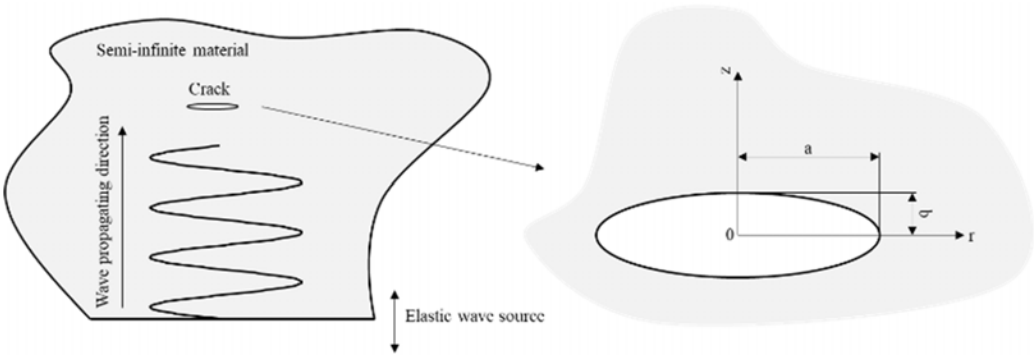

Fig. 4 In the semi-infinite material, a sinusoidal plane wave was propagating toward to the surface of the crack; the opened crack is modeled as an oblate spheroid

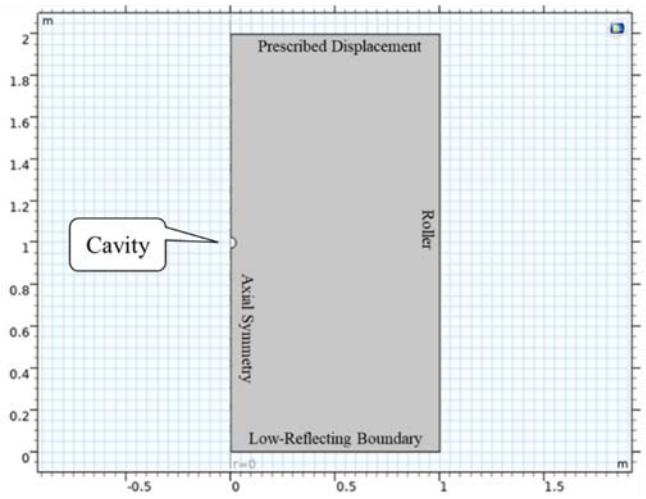

Fig. 5 Configuration of the boundary condition of the COMSOL model; axial symmetry is the axis of the cylinder; roller is the side wall of the cylinder; prescribed displacement at the top is the source of plane wave with the low-reflecting boundary at the bottom

Although there will be an acceptable discrepancy between the estimated and simulated resonance of the cavity (the estimated, (4), LDR frequency is 1.66 kHz for the spherical cavity with a radius of 6 mm embedded in steel with a Poisson's ratio of 0.3). When the Poisson's ratio is 0.4999, the simulated LDR frequency is 1.54 kHz. Vibration pattern of the local defect can be shown by the finite element simulation. When there is no cavity, there are no standing wave and reflection, and the vibration stress distribution of the cylinder should be uniform, as indeed demonstrated in Fig. 6 (a). When a spherical cavity is introduced in to the material, the stress on the intact area remains uniform while the stress around the sphere is elevated showing monopole distribution, Fig. 6 (b).

For simulating the resonance with different AR values, Young's modulus of the material is decreased to 0.2 GPa, and the radius of the sphere is increased to 2.5 cm in order to reduce the computation time. The simulated result agrees with the result in [15]. In the application process of VAM, the pump wave (low-frequency stress) will periodically change the shape of the defect varying AR. Knowing that the characteristic frequency of the cavity is dependent on AR, the resonance response of the crack will change accordingly, Fig. 7.

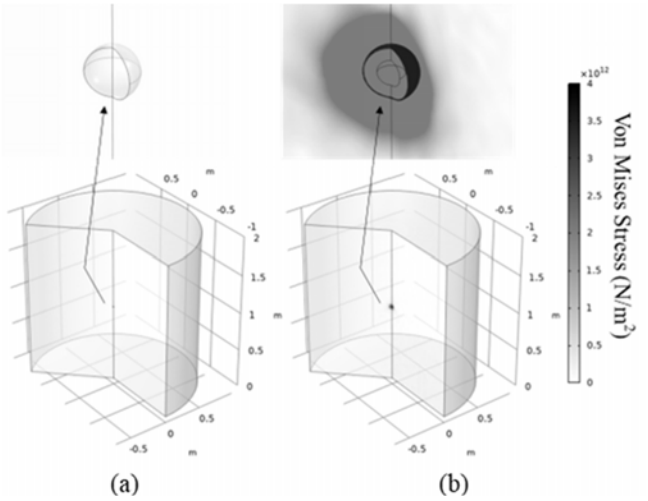

Fig. 6 Stress distribution of the intact cylinder (a), and the cylinder with the cavity (b)

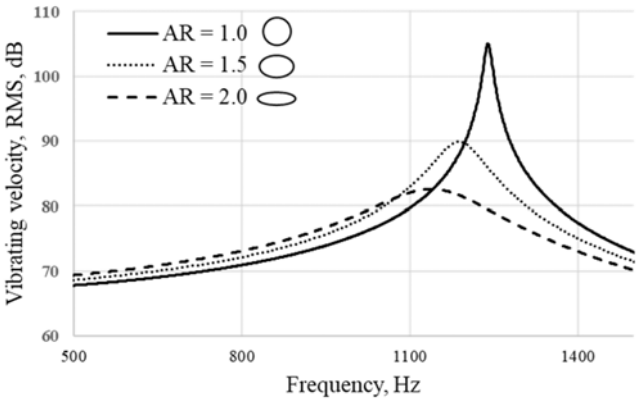

Fig. 7 The frequency response (vibrating velocity) of a point located on the surface of the cavity; The cavity with axis ratio AR = 1 (sphere), has highest resonance frequency than the cavities with greater AR (oblate spheroids)

B. LDR Vibro-Acoustic Frequency Modulation

Following LDR mass-spring model, we will utilize a generic mass-spring oscillator equation for the local strain, ξ:

$$m\ddot{\xi} + b\dot{\xi} + k\xi = A\cos(\omega t) \quad (5)$$

where b is the spring's damping coefficient, A is the amplitude of the incident carrier wave with the frequency ω.

LDR simulation results illustrated in Fig. 7 show that the resonance frequency is reduced with increased AR ratio which, in turn, is determined by the applied stress σ = Bcos(Ωt). This reduction in the resonance frequency can be explained by reduction in the cavity stiffness, therefore:

$$k_{eff} = k(\sigma) = k(\Omega t) \quad (6)$$

Since Ω ≪ ω, the stiffness changes are slow compared to period of oscillation 2π/ω. Additionally, we assume that these changes are small and proportional to low frequency dynamic function (vibration):

$$k(\Omega t) \cong k_0 - \Delta k \cos(\Omega t) \quad (7)$$

where $\Delta k \ll k_0$. Under the above assumptions, we can use the linear solution of (7) where amplitude and phase are functions of slow and small changing stiffness k(Ωt):

$$\xi(t) = \frac{A}{\sqrt{(k(\Omega t) - m\omega^2)^2 + b^2\omega^2}} \cos(\omega t - \phi(\Omega t)) \quad (8)$$

where,

$$\phi(\Omega t) = \tan^{-1}\left(\frac{b\omega}{k(\Omega t) - m\omega^2}\right) \quad (9)$$

As can be seen from (8) and (9), the LDR model with parametric stiffness (7) yields both amplitude and frequency modulations. These can be illustrated using amplitude and frequency responses as they are shifted right and left with frequency Ω, Fig. 8.

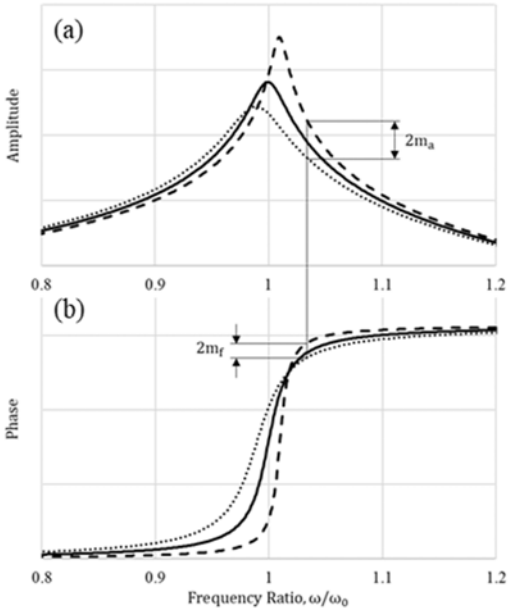

Fig. 8 Amplitude (a) and Phase (b) frequency responses, (8) and (9), as dynamic function cos(Ωt) varies from -1 (dotted line), to 0 (solid line), and to +1 (dashed line): $2m_a$ and $2m_f$ are respective amplitude and phase varying range (m_a and m_f are MI es) for a signal with carrier frequency ω (vertical solid line)

This simple model of the slow varying (modulating) frequency responses allows direct calculation of AM and FM modulating indexes, m_a and m_f, respectively, as illustrated in Fig. 8. This model also shows that the degree of AM and FM depends on carrier frequency proximity to the resonance frequency, f_{LDR} (3).

Fig. 9 (a) shows dependence of m_a and m_f as function of ω/ω_0. Interestingly, it shows dominant FM near and above the resonance frequency, while AM dominates below $0.8\omega_0$. It also shows extremely high modulations in the close proximity to the resonance. With increased damping, the FM dominance over AM spreads even more, while, as expected, MI are reduced in the resonance direct proximity, Fig. 9 (b).

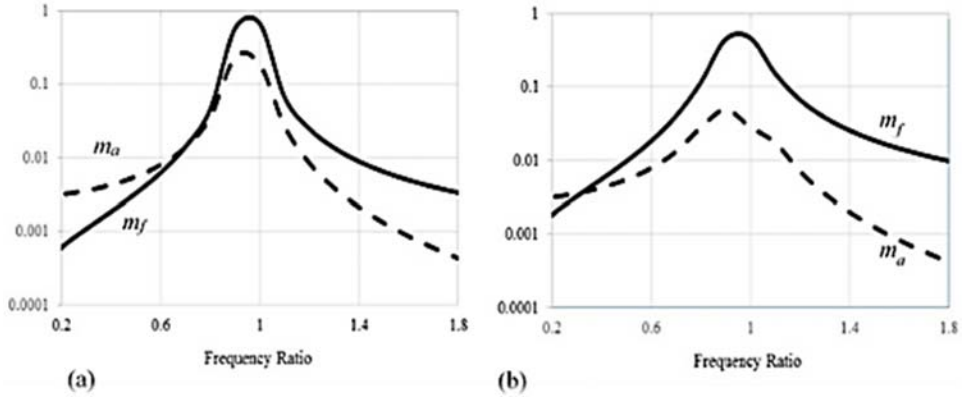

Fig. 9 AM and FM indexes vs. frequency ratio ω/ω_0 using direct calculations from frequency responses as shown in Fig. 8: In this exemplarity calculations the following parameter values were used: $M_{eff} = 0.001$, $k_0 = 35000$, $\Delta k = 0.1k_0$, $\Omega/2\pi = 10$Hz, $b = 0.3$ (a) and $b = 0.9$ (b)

II. Frequency Modulation due to Acoustoelasticity

Another possible mechanism of FM is due to the Acoustoelastic (AE) effect. The AE effect is the change in velocity of ultrasonic waves due to applied stress. Such stress-velocity relation may change when the higher order elastic coefficient of the structure changed by the imperfections such as micro- or macro-defects. Initially, this phenomenon was described for static stresses, [16], [17] and later was shown that it has also taken place for quasi-static or low frequency vibration: Dynamic Acoustoelasticity (DAE) [18].

DAE study demonstrated a noticeable change in the ultrasonic velocity near damaged region of the tested material and insignificant or no changes (for the level of applied vibration stresses) for undamaged (intact) regions. Neglecting a small hysteretic behavior observed in the tests, [2], the velocity change due to applied low frequency harmonic stress $\sigma = B\cos(\Omega t)$ can be approximated as follows:

$$c \cong c_0 + \Delta c \cos \Omega t \tag{10}$$

Here, the c_0 the ultrasonic velocity of the test structure without any external stress, Δc is the maximum velocity deviation attributed to the external dynamic stress.

We consider the one-dimensional case: the traveling acoustic (carrier) wave with the frequency ω propagates through a damaged region having length Δx. Within this region the sound speed is modulated as per (10), while outside the region the sound speed is constant and equal to c_0. Accordingly, the traveling wave can be described as:

$$\varepsilon \sim \cos\left[\omega\left(t - \frac{x-\Delta x}{c_0} - \frac{\Delta x}{c}\right)\right] \tag{11}$$

where c is defined by (10), ε is the strain, and x is the traveling distance.

Assuming $\Delta c/c_0 \ll 1$ and using the Tylor's expansion,

$$\frac{1}{c} = \frac{1}{c_0\left(1+\frac{\Delta c}{c_0}\cos \Omega t\right)} \cong \frac{1}{c_0} - \frac{\Delta c}{c_0^2}\cos \Omega t \tag{12}$$

Equation (11) can be re-written as following after substituting (12) into (11):

$$\varepsilon \sim \cos\left[\omega\left(t - \frac{x}{c_0} + \frac{\Delta x \Delta c}{c_0^2}\cos(\Omega t)\right)\right] \tag{13}$$

From (13), one can see that the traveling wave is frequency modulated with the MI:

$$m_f \cong \frac{\omega \Delta x \Delta c}{2c_0^2} \tag{14}$$

Using experimental data presented in [18], we can evaluate the possible frequency MI as per (14). DAE test of [18] was conducted using aluminum alloy A7075 sample having sound velocity $c_0 = 6250$ m/s, with the fatigue crack of length $\Delta x = 19$ mm: relative velocity deviation observed along the crack $\Delta c/c_0 \sim 0.001$ and as high as 0.003 at some locations. The probe wave frequency of DAE is much greater than VAM test. The high frequency used in [18] was 2 MHz and low vibration frequency was 7 kHz. DAE test measures the time of flight of the high frequency signal to measure ultrasonic velocity and its deviation due to low frequency stress. If this test would be configured as VAM test using the same high frequency signal as the carrier and low frequency as the modulating vibration, it would measure, (14), FM index $m_f \sim 0.02$ or -34 dB which is very high by VAM standards.

VAM tests typically use a low carrier and vibration frequencies; 100 kHz to 200 kHz for the carrier and 10 s to 100 s of Hz for the modulating vibration. Although lower carrier frequency should reduce the frequency MI as per (14), lower frequency vibration tends to produce higher stress potentially yielding greater velocity deviation $\Delta c/c_0$ especially for materials with lower sound speeds. Based on these considerations and the above estimate we can expect appreciable and detectable FM level in typical VAM tests.

III. Conclusion

The VAM method detects and monitors damage evolution from micro-defects to macro-cracks. There are numerous studies of VAM application to a variety of materials (metals, composites, ceramics, glass, etc.) and a variety of defects (fatigue damage, stress-corrosion cracks, delamination) [1]-[7]. Most of these studies utilize spectrum analysis to measure the MI defined as a ratio of the amplitudes of the spectral sidebands (product of modulation in the presence of a defect) to the carrier amplitude [1]-[7]. It is a common belief that the defects produce predominantly Amplitude Modulation. Preceding research [6] experimentally demonstrated that fatigue damage preceding formation of large cracks may produce predominantly Frequency Modulation, while contact-type nonlinearities produce primarily Amplitude Modulation.

The present work is an attempt to explain the Frequency Modulation by introducing two models: LDR and acoustoelastic FM model. Both models reveal the possibility of strong FM that could dominate over AM.

Acknowledgment

This work was partially supported by New Jersey Department of Transportation [contract # 17-60125].

References

[1] D. M. Donskoy and A. M. Sutin, "Vibro-acoustic modulation nondestructive evaluation technique," Journal of intelligent material systems and structures, 1998, pp. 9(9), 765-771

[2] L. Pieczonka, A. Klepka, A. Martowicz and W. J. Staszewski, "Nonlinear vibroacoustic wave modulations for structural damage detection: an overview," Optical Engineering, pp. 55(1), 011005., 2015.

[3] D. Donskoy, A. Chudnovsky, A. Zagrai and E. Golovin, "Micro-Damage Evaluation and Remaining Fatigue Life Assessment with Nonlinear Vibro-Modulation Technique," AIP Conference Proceedings, pp. Vol. 1022, No. 1, pp. 509-512, 2008, June.

[4] T. Ooijevaar, M. D. Rogge, R. Loendersloot, L. Warnet, R. Akkerman and T. Tinga, "Vibro-acoustic modulation–based damage identification in a composite skin–stiffener structure," Structural health monitoring, pp. 15(4), 458-472, 2016.

[5] D. M. Donskoy, "Nonlinear acoustic methods, encyclopedia of structural health monitoring," 2009, pp. 321-332.

[6] D. M. Donskoy and M. Ramezani, "Separation of amplitude and frequency modulations in vibro-acoustic modulation nondestructive testing method," in Proceedings of Meetings on Acoustics 21ISNA, 2018.
[7] H. F. Hu, W. J. Staszewski, N. Q. Hu and R. Jenal, "Crack detection using nonlinear acoustics and piezoceramic transducers—instantaneous amplitude and frequency analysis," Smart materials and structures, pp. 19(6), 065017., 2010.
[8] I. Solodov, J. Bai and G. Busse, "Resonant ultrasound spectroscopy of defects: case study of flat-bottomed holes," Journal of Applied Physics, vol. 113(22), p. 223512, 2013.
[9] I. Solodov, M. Rahammer and N. Gulnizkij, "Highly-sensitive and frequency-selective imaging of defects via local defect resonance," The e-Journal of Nondestructive Testing, vol. 19, p. 12, 2014.
[10] I. Solodov, "Resonant acoustic nonlinearity of defects for highly-efficient nonlinear NDE," Journal of Nondestructive Evaluation, vol. 33(2), pp. 252-262, 2014.
[11] J. Segers, M. Kersemans, S. Hedayatrasa, J. Calderon and W. Van Paepegem, "Towards in-plane local defect resonance for non-destructive testing of polymers and composites," NDT & E International, vol. 98, pp. pp.130-133, 2018.
[12] S. I. and K. M., "Local defect resonance of a through-thickness crack," Ultrasonics, vol. 118, p. 106565, 2022.
[13] W. Weaver Jr, S. P. Timoshenko and D. H. Young, Vibration problems in engineering, John Wiley & Sons, 1990.
[14] L. D. Landau and E. M. Lifshitz, Theory of elasticity, Butterworth-Heinemann, 1984.
[15] Calvo, David C., Abel L. Thangawng, and Christopher N. Layman. "Low-frequency resonance of an oblate spheroidal cavity in a soft elastic medium." The Journal of the Acoustical Society of America 132.1 (2012): EL1-EL7.
[16] D. S. Hughes and J. L. Kelly, "Second-order elastic deformation of solids," Physical review, pp. 92(5), 1145, 1953.
[17] Norris, A. N. (2007). "Small-on-Large Theory with Applications to Granular Materials and Fluid/Solid Systems" (PDF). In M. Destrade; G. Saccomandi (eds.). Waves in Nonlinear Pre-Stressed Materials. CISM Courses and Lectures. Vol. 495. Springer, Vienna.
[18] J. Riviere, M. C. Remillieux, Y. Ohara, B. E. Anderson, S. Haupert, T. J. Ulrich and P. A. Johnson, "Dynamic acousto-elasticity in a fatigue-cracked sample," Journal of Nondestructive Evaluation, pp. 33(2), 216-225., 2014.